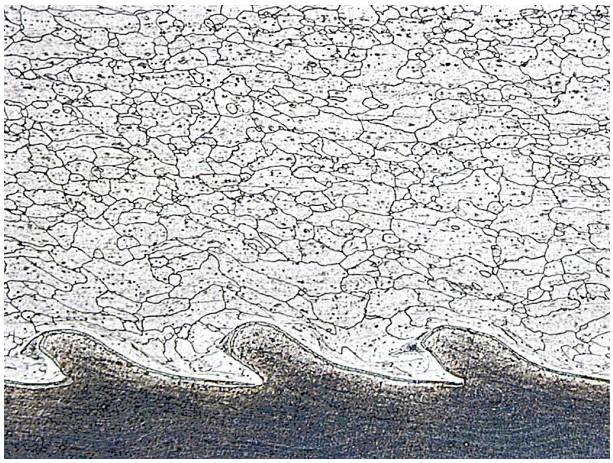

Analysis on the effectiveness of the weldability window in predicting results for explosive welding

DUARTE MIGUEL GONÇALVES PELADINHO
(Licenciatura em Engenharia Mecânica)

Dissertação para obtenção do grau de Mestre em Engenharia Mecânica, na Área de Especialização de Manutenção e Produção

Orientadores:
Doutor Ivan Rodolfo Pereira Garcia de Galvão
Doutor Gustavo Henrique Senna de Freitas Ligeiro de Carvalho
Doutor Rui Manuel Ferreira Leal

Júri:
Presidente: Doutora Maria Amélia Ramos Loja
Vogais:
Doutor Altino de Jesus Roque Loureiro
Doutor Ivan Rodolfo Pereira Garcia de Galvão

Novembro 2025

Analysis on the effectiveness of the weldability window in predicting results for explosive welding

DUARTE MIGUEL GONÇALVES PELADINHO
(Licenciatura em Engenharia Mecânica)

Dissertação para obtenção do grau de Mestre em Engenharia Mecânica, na Área de Especialização de Manutenção e Produção

Orientadores:
Doutor Ivan Rodolfo Pereira Garcia de Galvão, ISEL/IPL
Doutor Gustavo Henrique Senna de Freitas Ligeiro de Carvalho, DIEF/UNIFI
Doutor Rui Manuel Ferreira Leal, ESAD.CR/IPLeiria

Júri:
Presidente: Doutora Maria Amélia Ramos Loja, ISEL/IPL
Vogais:
Doutor Altino de Jesus Roque Loureiro, UCoimbra
Doutor Ivan Rodolfo Pereira Garcia de Galvão, ISEL/IPL

Novembro 2025

Acknowledgements

I would like to express my sincere gratitude to my supervisors, Professor Ivan Galvão, Professor Gustavo Carvalho, and Professor Rui Leal, for their guidance, constructive feedback, and steady support throughout this work. Their expertise and high standards greatly improved this dissertation.

I am deeply thankful to my parents for their unwavering support and the many sacrifices that made this journey possible. To my grandmother, whose affection and belief in me have been a constant source of strength, I offer a special thank you.

Statement of integrity

I declare that this dissertation is the result of my personal and independent research. Its content is original, and all sources listed in the bibliographic references were consulted and are duly mentioned in the text. I further declare that all scientific and technical references relevant to the development of the work are duly cited and included in the bibliographic references.

The author

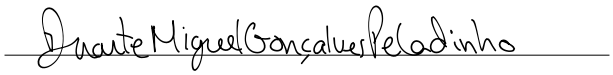

Lisbon, 06 November 2025

Analysis on the effectiveness of the weldability window in predicting results for explosive welding

Abstract

Explosive welding (EXW) is a solid-state joining process that relies on controlled detonation to achieve metallurgical bonding between similar or dissimilar materials. Its advantages include the ability to combine metals with large differences in melting point and thermal conductivity, the near absence of a heat-affected zone, and the potential for producing large-scale joints. Nevertheless, the main limitation of EXW remains the lack of a reliable theoretical framework capable of predicting weld quality. To address this limitation, the weldability window was introduced as a graphical tool relating collision velocity and collision angle to the likelihood of a successful weld. Although widely used, this model often fails to reproduce experimental results, mainly due to the diversity of proposed equations, the boundary conditions considered during their development, and the incomplete understanding of interfacial mechanisms such as wave formation and jetting.

The objective of this work is to analyse the effectiveness of the weldability window in predicting the outcomes of explosive welding by reviewing and comparing the most relevant theoretical formulations with experimental results available in the literature. The examination of these approaches highlights the assumptions behind each model and reveals important divergences regarding their applicability to different materials and welding conditions. The analysis shows that current formulations contain inconsistencies that restrict their predictive capability, resulting in discrepancies between theoretical boundaries and actual weld behaviour. These limitations emphasize the need for further refinement of the weldability window in order to provide a more accurate and reliable framework for assessing the occurrence of successful welds in explosive welding processes.

Keywords

Explosive welding; Weldability window; Solid-state joining

Análise da eficácia da janela da soldabilidade na previsão de resultados em soldadura por explosão

Resumo

A soldadura por explosão (EXW) é um processo de união em estado sólido que recorre a uma detonação controlada para promover a ligação metalúrgica entre materiais semelhantes ou dissimilares. As suas principais vantagens são a possibilidade de combinar metais com diferenças significativas de ponto de fusão e condutividade térmica, a quase ausência de zona termicamente afetada e o potencial para unir partes de grandes dimensões. Contudo, a maior limitação da EXW continua a ser a inexistência de um modelo teórico fiável capaz de prever a qualidade da união. Assim, foi desenvolvida a janela de soldabilidade, uma ferramenta gráfica que relaciona a velocidade de colisão e o ângulo dinâmico com a probabilidade de obtenção de uma soldadura bem-sucedida. Apesar da sua ampla utilização, este modelo frequentemente não é fiel aos resultados experimentais, devido à diversidade de equações propostas, às condições específicas em que foram obtidas e à compreensão ainda incompleta de alguns fenómenos interfaciais, como a formação de ondas e a formação do jato.

O objetivo deste trabalho consiste em analisar a eficácia da janela de soldabilidade na previsão dos resultados da soldadura por explosão através da revisão e comparação das formulações teóricas mais relevantes com resultados experimentais disponíveis na literatura. A avaliação destas abordagens evidencia as premissas em que cada modelo assenta e revela divergências significativas relativamente à sua aplicabilidade a diferentes materiais e condições de soldadura. A análise demonstra que as formulações atuais apresentam inconsistências que limitam a sua capacidade preditiva, originando discrepâncias entre os limites teóricos e o comportamento real das soldaduras. Estas limitações reforçam a necessidade de um maior refinamento da janela de soldabilidade, de modo a fornecer uma estrutura mais precisa e fiável para a avaliação da ocorrência de soldaduras bem-sucedidas em processos de soldadura por explosão.

Palavras-chave

Soldadura por explosão; Janela de Soldabilidade; Soldadura em estado sólido

List of Figures

List of Tables

List of Symbols

Latin

a	Interfacial wave amplitude	m
C_b	Bulk sound speed in base plate	m/s
C_f	Bulk sound speed in flyer plate	m/s
C_p	Specific heat capacity	J/(kg·℃)
E	Young's modulus	Pa
f	Empirical factor in upper-limit model	–
G	Shear modulus	Pa
h_b	Base plate thickness	m
h_f	Flyer plate thickness	m
HV_b	Vickers hardness of base	–
HV_f	Vickers hardness of flyer	–
I_d	Pressure-deforming pulse	kNs/m^2
K	Thermal conductivity	W/(m·℃)
k	Surface cleanliness coefficient (0.6–1.2)	–
KE	Kinetic energy	J
N	Material-dependent constant ($\sim$0.11)	–
$p_{\max}$	Maximum pressure at collision point	Pa
R	Explosive ratio	–
R_c	Reynolds number	–
r_{bi}	Base inner radius (cylindrical config.)	m
r_{fi}	Flyer inner radius (cylindrical config.)	m
r_{fo}	Flyer outer radius (cylindrical config.)	m
T_m	Melting temperature	℃
t_1	Process time scale in thermal criterion	s
t_2	Process time scale in melting criterion	s
t_p	Characteristic plastic deformation time	s
t_s	Solidification/heat removal time	s
t_w	Plastic deformation duration	s

$\tilde{m}$	Average mass per unit area of plates	kg/m^2
V_c	Collision (welding point) velocity	m/s
$V_{i,cr}$	Critical impact velocity	m/s
V_p	Flyer plate impact velocity	m/s
W_2	Energy spent on metal deformation	J/m^2
W_2^{cr}	Critical deformation energy threshold	J/m^2
ΔKE	Loss of kinetic energy per unit area of the plates	J/m^2

Greek

α	Thermal diffusivity	m^2/s
β	Collision angle	deg or rad
β'	Outgoing angle after impact	deg or rad
σ_b	Ultimate tensile strength	Pa
σ_y	Yield strength	Pa
ν	Poisson's ratio	–

Acronyms

EXW Explosive Welding.

FW Fusion Welding.

HEL Hugoniot Elastic Limit.

MAG Metal Active Gas.

MIG Metal Inert Gas.

SSW Solid-State Welding.

TIG Tungsten Inert Gas.

VFAW Vaporizing Foil Actuator Welding.

WIF Wave Interface Factor.

Summary

Chapter 1

Introduction

Chapter 1 sets the context and motivation for studying explosive welding. It briefly reviews main joining methods, distinguishes fusion from solid-state processes, and places explosive welding among them. The chapter outlines basic process features, common setups, advantages and limits, and notes key historical steps. Finally, it ends with the motivation, objectives, and the structure of the work.

1.1 Contextualization of the topic

The continuous advances in many fields of engineering create a high demand for new and improved materials with stricter and more individual characteristics. Some requirements can only be met by materials that are far too expensive for the given application or can't be met at all by any known material. The joint of different materials presents as a solution for this problem, allowing engineers to hand pick the desired final characteristics of a material for a given application.

The different techniques of combining different materials can be divided in two main categories: mechanical joining and bonding. Mechanical joining uses connectors like rivets or bolts to join different materials. The main advantages of this method are the ability to combine different kinds of material, its low cost, ease of implementation, and the absence of thermal gradients and, for temporary fixings, ability to disassemble structures as required for repair and maintenance. However, the use of mechanical fasteners adds weight to the assembly, creates an uneven distribution of forces of the materials as the holes created for the fasteners might lead to stress concentrations and can't by itself guarantee a seal on applications for gases and liquids.

Bonding refers to the joining of materials by use of an adhesive or through a welding process. An adhesive is any substance that promotes bonding between two materials, like glue and cement. This type of joining leads to lighter assemblies, allow for the joining of different kinds of materials and thin sheets and do not require or produce very high temperatures. However, a good adhesive bond requires a thorough clean of the surfaces and the bond does not present a high resistance to shear stresses for temperatures above 100 °C.

The other bonding technique refers to welding which was defined by Messler [1] as a process in which materials of the same fundamental type or class are brought together and caused to join (and become one) through the formation of primary (and, occasionally, secondary) chemical bonds under the combined action of heat and/or pressure where an intermediate or filler material may or may not be used. Furthermore, welding is used to join parts but does so by joining materials which means that the properties of the parts (material, part shape, part dimensions) will matter to define the welding technique to be used and its parameters.

The main advantages of welding are the structural integrity of the joining and efficiency, wide range of applications and materials that can be welded, leak tight joints for liquid and gaseous applications and its moderate cost. However it makes it impossible to disassemble joints without destruction of parts and the utilization of heat may negatively impact the materials.

There are many different ways of classifying the various welding processes. For this work the chosen classification is based on the type of energy, heat or pressure, that is responsible for bonding or, indirectly, the quantity of material melting [2]. The two following groups can be considered: Fusion Welding (FW) and Solid-State Welding (SSW). FW is a type of welding where the two metal surfaces being joined are melted by the application of heat. Due to the melting, the contaminant surface films can either be brought to the surface or dissolved within the molten metal, resulting in clean surfaces. Examples of this are Metal Inert Gas (MIG)/Metal Active Gas (MAG), Tungsten Inert Gas (TIG) and Oxyacetylene Welding. SSW is a type of welding that relies primarily on pressure and where heat may still be involved and some local melting can still occur but it is not the principal responsible for joining the materials [3]. Examples of this are Friction Stir Welding, Roll Bonding, Ultrassonic Welding, Magnetic Pulse welding, Vaporizing Foil Actuator Welding and Explosive Welding (EXW) or Explosion Welding. EXW is a SSW that uses the sudden energy released by means of a controlled detonation of explosives to bond two or more pieces of similar or dissimilar metals or alloys. As described by Crossland [4], while welding has been around for thousands of years in the form of forging and soldering, dating back to 3000 B.C., only in the nineteenth century with the discovery of batteries, generators, oxygen and acetylene were developed other welding techniques.

This welding process is one of the most useful and hence its growing importance. Next are listed some of its advantages and limitations [5–8].

Advantages:

- Low cost welding process;
- Ability to weld large simple geometries quickly;
- Almost total lack of heat affected zone and therefore less probability of warping or affecting the materials properties;
- Allows for the joining of dissimilar materials with great differences in melting point and thermal conductivity;
- The weld interface is usually stronger than the weaker of the parent materials.

Limitations:

- Only suitable for a small number of simple geometries;
- The use of an explosive can be dangerous;
- The materials being welded must possess sufficient ductility to endure the impact.

1.2 Motivation

Explosive welding has been growing in importance in the welding community during the last few years due to its advantages as the capacity to join dissimilar materials, its absence of a thermally affected zone, and its ability to weld parts of considerable size, even though only for simple geometries, to name a few. However, one of the main problems with explosive welding is the lack of a theoretical model that is capable of accurately predicting the quality of a weld. Therefore, the available options in the past were to perform a significant amount of welds until one with the desired characteristics is obtained, which can be labour intensive, expensive and time consuming, or to hire an experienced weld technician who could pick the best parameters from his/her empirically acquired knowledge, which can prove difficult to do and also expensive. As a solution to this problem, the weldability window was created to provide theoretical predictions based on different parameters. Nevertheless, the results from this model often do not match the experimental results. This can be explained by several facts: the current window limits are defined by formulas that were obtained by different authors, other formulas were defined in particular settings and conditions and other for similar materials which does not represent the welding conditions of other materials or pairs of materials, the phenomena that the formulas try to describe are in some cases still not fully understood, or there is still no general scientific consensus.

1.3 Objectives

The objective of this work is to analyse the effectiveness of the weldability window in predicting the outcomes of explosive welding by reviewing and comparing the most relevant theoretical formulations with experimental results available in the literature.

1.4 Structure of document

This document is structured as follows: Chapter 1 is an introduction where the importance of explosive welding is outlined, as well as a brief overview on material joining leading up to explosive welding and its origins, its advantages over other methods followed by a an explanation on the motivation and objectives of the dissertation itself. Chapter 2 starts with a brief contextualization on the weldability window, and then the literature review for each of the 4 limits that define the weldability window. In Chapter 3 an analysis is made of experimental data from the literature to build a rough predictor of weld quality using collision velocity and kinetic energy. It then revisits the equations from Chapter 2, compares their predictions with available experimental results and notes the limitations of each. Chapter 4 presents the conclusions of the dissertation and suggests directions for future work.

Chapter 2

Literature Review

According to Crossland [9] and Carpenter and Wittman [10] the beginnings of Explosive Welding date back to the First World War when it was observed that fragments from bombs or sheels would often bond to other metals parts after impact [11]. The first known document on EXW was written by Carl [12] that noticed the phenomenon when conducting experiments in which a detonator was sepatared by two brass shims and found the shims would become welded and its interface would present interfacial waves. Several independent researchers then started more in-depth studies of EXW: Philipchuk [13] also observed the effect when explosively forming an aluminum U-channel in a steel die. Around the same time, Rinehart et al. [14, 15] when working on explosive presses for powder compaction noticed that if the plates were not in a parallel configuration but instead in an oblique configuration, the plates would become explosively welded together. Further advancements were made in the 1960s with contributions from researchers such as Holtzman and Rudershausen [16], Deribas et al. [17], Zernow et al. [18] and Bahrani and Crossland [19]. It is now recognized as a practical joining process with many applications with even NASA [20, 21] recognising it as being a feasible and practical joining process with immense potential for assembly of structures in space. Due to its nature, EXW can only be used on a handful of simple geometries. The two most common are the flat surfaces parallel and the oblique configurations [22, 23] as seen in Figures 2.1a and 2.1b.

In the first case, two flat plates are setup at constant stand-off distance, being one the base plate and the other the flyer plate. In this case, the detonation velocity V_d and the collision point velocity V_c are the same. The angle between the base plate and the deformed flyer plate is the dynamic angle of collision β.

As for the second case, the stand-off distance increases as the distance to the detonator increases. The choice between another is mainly based on the type of explosive to be used since on the parallel configuration $V_c = V_d$ and if the explosive has a detonation velocity too high the quality of the weld may be hindered [24]. Another useful configuration is the cylindrical as seen in Figure 2.2. In this configuration two coaxial cylinders are setup with a stand-off distance between them and the explosive charge on the inside of the smaller diameter cylinder. If looking at the process from a section view a resemblance to the parallel configuration can be seen and both the physics and the parameters can be transposed from one another [5, 25].

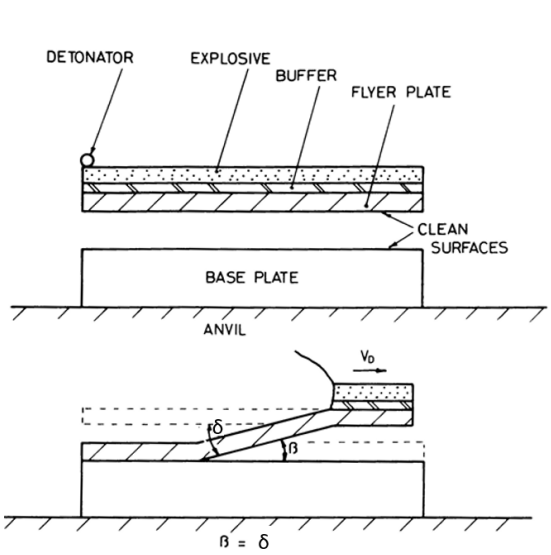

(a) Parallel configuration. Adapted from [5].

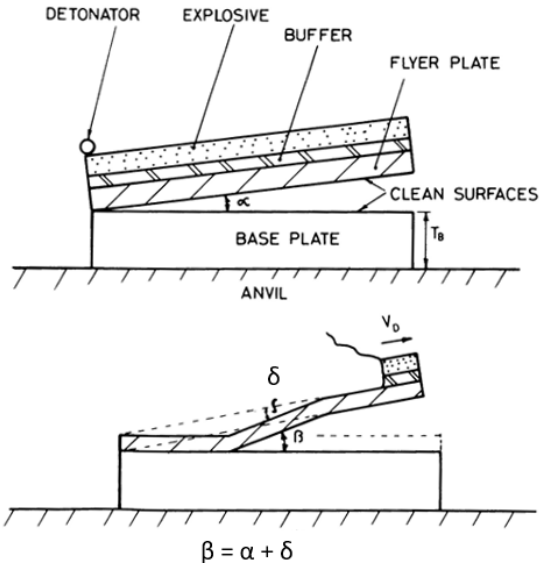

(b) Oblique configuration. Adapted from [5].

Figure 2.1 Types of planar configurations. Adapted from [5].

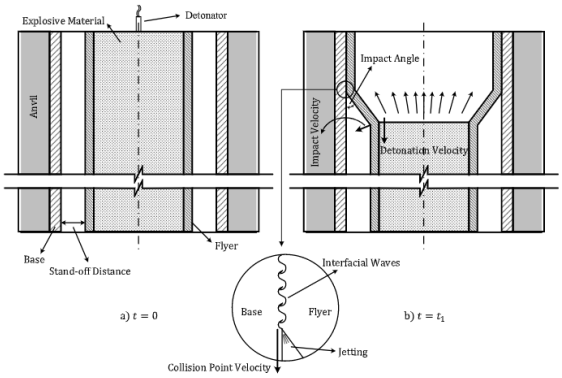

Figure 2.2 Cylindrical configuration. Adapted from [25].

The weldability window is a graphical representation of the range of process parameters within which explosive welding can successfully occur. It aims to indicate whether a weld will be effective or not by means of relating the collision point velocity V_c to the dynamic angle of collision β against equations that define those parameters limits, i.e, if the point defined by a certain V_c and β is located inside the "window", then the probability for a quality weld is high [26, 27]. The first attempt at definition of a weldability window was made by Wittman et al. [28] and is still the most widely accepted. A representation of the weldability window can be seen on Figure 2.3. The window is created by limits that can are identified by its position on the graphic - Left Limit, Lower Limit, Upper Limit and Right Limit.

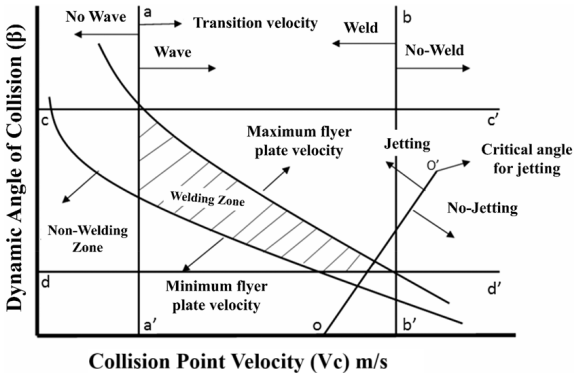

Figure 2.3 Weldability window. Adapted from [27].

2.1 Left Limit

The left limit represents the transition from a straight to a wavy interface. The formation of waves in the interface is a common phenomenon on explosive welds and considered indicative of a good weld, even though Carvalho et al. [29] showed that smooth interfaces can also have good mechanical properties as long as there is not a continuous layer of intermetallic compounds. The process of wave formation remains a topic of ongoing discussions within the welding community.

Cowan et al. [30] are the authors of one of the most well-known models and the one that is still the most often used to describe the left limit. The authors noticed the visual similarity between the wavy bond zone (Figure 2.4a) and the von Kármán vortex streets in fluid flow around an obstacle above a certain Reynolds number (Figure 2.4b).

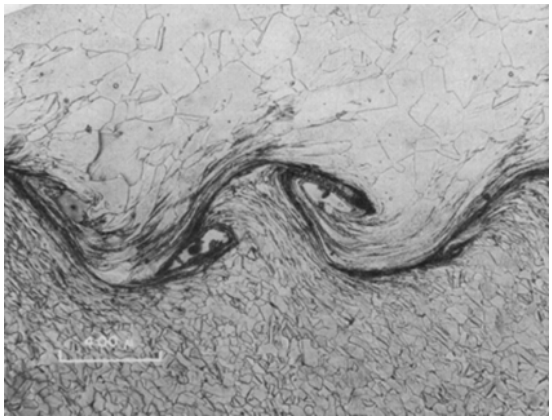

(a) Bond zone of nickel on steel clad made at a collision velocity of V_C = 2500m/s. Adapted from [30].

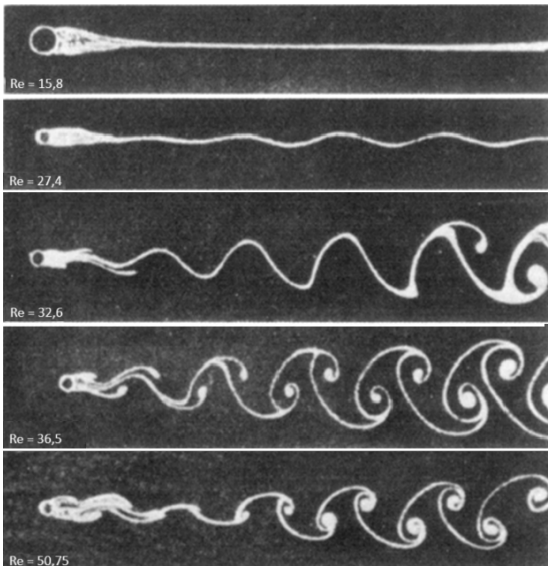

(b) Photographs of fluid flow behind cylinders at increasing values of the Reynolds number, R. Adapted from [30].

Figure 2.4 Wavy interface phenomenon. Adapted from [30].

Given that the pressure near the collision point is very high and far exceeds the metal yield strength, the rate of plastic deformation in this area will be extremely high, and the materials can be considered to behave liquid-like. Therefore, it was suggested that the boundary line between a smooth and a wavy interface could be approximated by the superposition of the Newtonian liquid behaviour and that of elastic-plastic material as represented on Figure 2.5. According to theirs and previous authors [17, 31] observations that the wave amplitude is strongly dependent on collision angle and independent of collision velocity the Reynolds number should be formulated in terms of the static strength of the metals. The equation for the transition R_c then becomes:

$$R_c = \frac{(\rho_f + \rho_b)V_c^2}{2(HV_f + HV_b)} \tag{2.1}$$

ρ_f, ρ_b, HV_f and HV_b are the densities and Vickers hardnesses for the flyer plate and base plate, respectively, and V_c is the collision point velocity. The authors further state that the transition from a straight to a wavy interface should occur at the same transition Reynolds for different systems. On their experiments, with the collision angle kept constant at 12 degrees, an average Reynolds $R_c \approx 10.6$ was obtained.

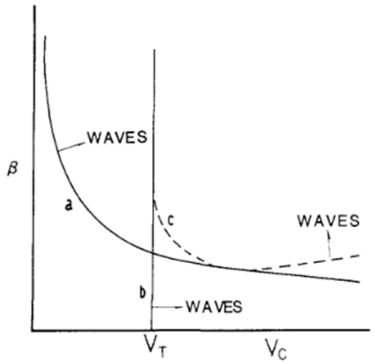

Figure 2.5 Theoretical boundaries of wave formation for collisions (a) of flat streams of Newtonian liquids, and (b) of flat plates of elastic-platic solids. (c) Typical observed boundary of wavy bond zones in metal cladding. Adapted from [30].

Jaramillo et al. [32] argued that even though Cowan et al. [30] suggested that the transition from a smooth to a wavy interface could be approximated by the superposition of the newtonian liquid behaviour and that of elastic-plastic material, they used a straight line, therefore independent of the collision angle and contradicting their previous sugestion. This limit would only represent the transition for an elastic-plastic material and therefore does not agree with the hydrodynamic analogy they had established. The authors also pointed another flaw on the hydrodynamic analogy. This analogy although plausible for the collision point region, cannot be extended to the rest of the interface as the plates regain their solid characteristics as soon as they leave that area and would stop exhibiting fluid-like behavior. In real fluids, the waves only reach a stable configuration after a certain distance from the obstacle.

Jaramillo et al. [32] carried out several experiments using a gas gun with varying collision angles. These experiments were carried out for systems comprising of copper/copper, mild steel/mild steel and aluminum alloy 2024/aluminum alloy 2024, with the flyer plates having a thickness of 3.2 mm for all three systems. The results were plotted and equations that fitted the plots were obtained for each system. When all the data for the three systems was combined, the authors managed to derive a general relationship between the elastic-plastic constant and the collision angle, β, (Equation 2.2) being the terms inside the parentheses the standard deviation and the equation having a correlation factor of 0.9853.

$$KE = 93.02(\pm 9.62) - 13.45(\pm 2.06)\beta + 0.71(\pm)\beta^2 - 0.012(\pm 0.03)\beta^3 \tag{2.2}$$

Minding the previous formula, a gradual transition therefore occurs inside a transition zone instead of a sharp transition. The authors also noted from their experiments that the transition from a waveless to a wavy interface was influenced by the thickness of the thinner material being welded.

Vivek et al. [33] utilized an accurate, low-cost, lab-scaled process developed by Vivek et al. [34] for determining the optimal collision angles and velocities for collision welding. This process, named Vaporizing Foil Actuator Welding (VFAW), uses the pressure created from an electrically driven rapid vaporization of a thin foil of aluminium to propel the flyer plate against the base plate. The materials to be welded were copper and titanium measured to be 90 HV and 170 HV, respectively. The 6.3 mm copper plates served as the base plates which were machined with various V-shaped grooves at angles varying from 8° to 28° at intervals of 4° (Figure 2.6a). These angled grooves served to provide the collision angles instead of angling the flyer plate relatively to the base plates as shown in Figure 2.6b. The 0.5 mm thick titanium flyer plate was placed at a 1.6 mm stand-off distance from the base plate. The capacitor bank was charged with 3 kJ and from 4 kJ to 12 kJ at intervals of 2 kJ, therefore, varying the propulsion felt by the flyer plate, as if, R was being increased.

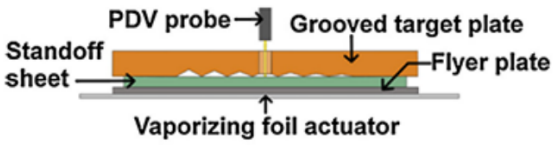

(a) Experimental set up for the welding window determination using VFAW. Adapted from [33].

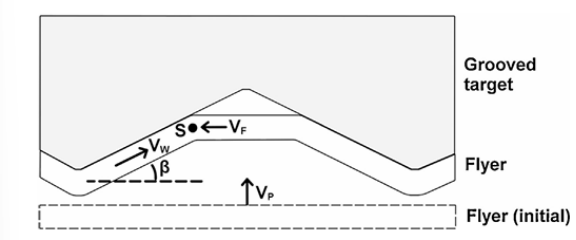

(b) A schematic representation of the progress of welding process. S is the collision point which moves at a velocity Vw as the weld progresses. Adapted from [33].

Figure 2.6 Setup and representation for VFAW. Adapted from [33].

Fitting a cubic polynomial to the data yielded the following equation.

$$KE = 175.53 - 15.995\beta + 0.5174\beta^2 - 0.0053\beta^3 \tag{2.3}$$

This equation presents with a correlation factor of 0.9174 and resembles Equation 2.2 as in both are a cubic polynomial, however the constant and coefficients differ. This difference could be attributed to the fact that Jaramillo et al. [32] studied systems with the same material for base and flyer plates and Vivek et al. [33] studied systems with different materials. Also, as mentioned by Jaramillo et al. [32] the thickness of the plates can affect the transition zone.

Salem et al. [35] studied the welding process on multiple plates colliding in free flight. They described the process as a progressive multiple collision of two plates of different thicknesses. On their studies they performed two-layered experiments to weld commercially pure aluminium plates of different thicknesses freely in air. As for the plates, the flyer plates had a thickness of 4.8 mm and the base plates ranged from 0.91 to 17.3 mm. On a later stage they performed multilayered welding experiments for various metals, including aluminium, copper and steel, with plate thickness ranging from 0.4 mm to 6.8 mm. The number of layers varied and so did both the top stand-off distance and the interlayer stand-off distance.

On these experiments it was found that the waves would diminish in size as the interface position number increased, i.e, the further the given plate was from the driver plate, the smaller the interface waves would be in amplitude as represented in an example in Figure 2.7.

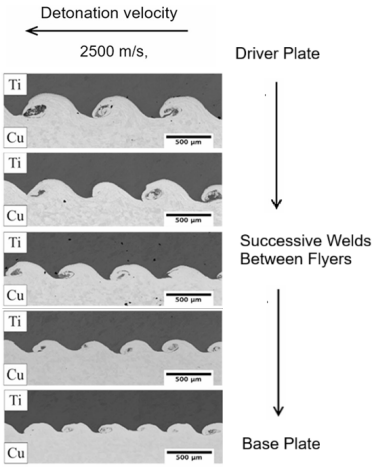

Figure 2.7 Example of variation of amplitude as described by [35]. Adapted from [36].

The last interface was heavily dependent on how the last layer was supported. If the last plate was also freely in the air, then as before, there is further reduction in wave amplitude, however, in the presence of a base plate, the last interface would present significantly bigger wave amplitudes.

The authors then described the loss of kinetic energy of the system per unit area of the plates due to the collision as per equation 2.4:

$$\Delta KE = \frac{1}{2}\rho_f V_{P_f}^2 \left[1 - \frac{h_f\rho_f}{h_f\rho_f + h_b\rho_b} \times \left(\frac{cos(\beta/2 - \beta')}{cos\beta'/2}\right)^2\right] \tag{2.4}$$

Or alternatively per equation 2.5:

$$\Delta KE = 2V_C^2[h_f\rho_f(sin^2\beta/2 - sin^2\beta'/2) - h_b\rho_b sin^2\beta'/2] \tag{2.5}$$

ΔKE is loss of kinetic energy per unit area of the plates, h_f, ρ_f and V_{P_f} are the thickness, density and velocity of the flyer plate, h_b, ρ_b and V_{P2} are the thickness, density and velocity of the next plate, β is the angle at which the flyer plate travels to the next plate and β' is the angle that both plates make with the horizontal axis after colliding as shown in Figure 2.8.

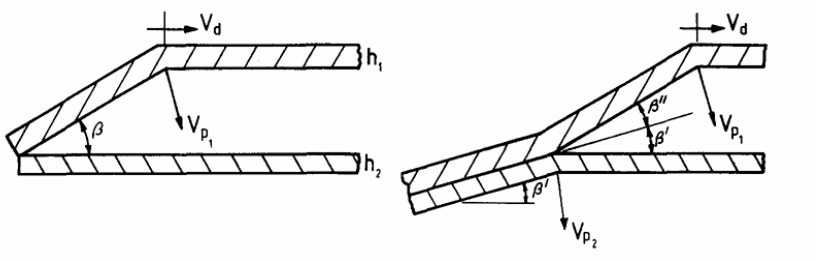

Figure 2.8 Schematic diagram showing the welding of two plates in free flight. Adapted from [35].

From equation 2.5, considering $\beta' = 0$, equation 2.6 then describes the loss of kinetic energy per unit area of the plates for a two-plate system.

$$\Delta KE = 2V_C^2 h_f\rho_f(sin^2\beta/2) \tag{2.6}$$

This equation does not explicitly define the critical value for the transition from a waveless to a wavy interface but could, potentially, be used to obtain it through an experimental procedure as perform by Jirdehi et al. [25] and explained next.

Jirdehi et al. [25], following the developments of Salem et al. [35] on the solid mechanics approach, set out to establish an analytical model for predicting the dimensions of the interfacial waves produced in explosive welding, specifically, for coaxial cylinders configurations. The authors also aimed to consider the effects of flyer geometry on the transition phenomenon in accordance with Jaramillo et al. [32] observation that the thickness of the plates also affected the transition zone. To accomplish the previous, the authors re-traced the steps Salem et al. [35] took in obtaining Equations 2.5 and 2.6 but considering the cylindrical configuration and the result was Equation 2.7.

$$KE = \rho_f V_C^2 \left(\frac{r_{fo}^2 - r_{fi}^2}{r_{bi}}\right) sin^2\frac{\beta}{2} \tag{2.7}$$

r_{fo}, r_{fi} and r_{bi} represent the outer and inner radius of the flyer plate and the inner radius of the base plate. With resource to computer simulations of the Finite Element and the Smoothed-Particle Hydrodynamics methods and utilizing experimental data from explosive welding of stainless-steel 316L (flyer) to carbon steel CK22 (base) tubes, the Equation 2.7 was validated. A total of 14 numerical models was created. All the tubes measured 100 mm in length, Models No.1 to No.8 used thin-walled flyer tubes with a thickness of 1.65 mm and mass of 129 g, while the Models No.9 to No.14 used thick-walled flyer tubes with a thickness of 3.38 mm and a mass of 250 g. Of these experiments, Models No.5, No.10 and No.11, even though they were located within the allowable boundaries of the weldability windows, presented completely smooth interfaces. By using equation 2.7 to calculate the kinetic energy lost for the different samples, the authors managed to plot this data against the wavelength of the waves in the interface. This allowed them to observe that the wavelength, λ of the waves decreases somewhat linearly with the decrease in lost kinetic energy, up to a point. As soon as the KE reduces below a critical value, the linear behaviour is interrupted and λ increases rapidly as seen in Figure 2.9. This critical value was calculated at $KE = 515$ J/cm^2 for the studied systems. This value was obtained based on multiple experiments with different thickness cylinders but always considering the same materials aforementioned and can vary depending on the materials used. The authors further conclude that the determination of KE is of high significance for the characterization of the wavy-smooth transition process as this transition occurs at a critical value of KE.

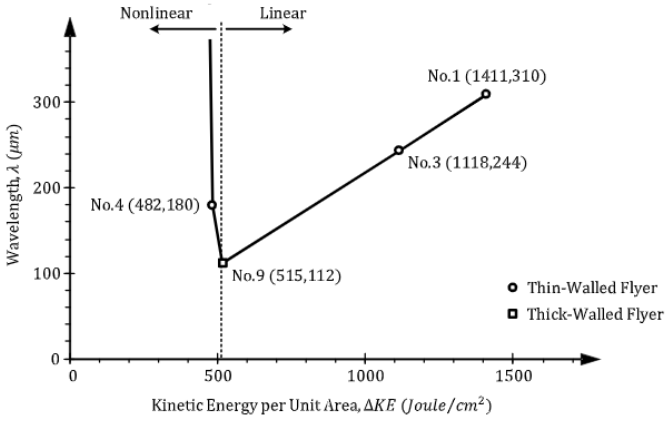

Figure 2.9 Diagram of wavelength to the kinetic energy lost per unit area. Adapted from [25].

Loureiro et al. [7] reported the work of Carvalho et al. [37] which reviewed numerous experiments and found that wave formation at the weld interface depends strongly on the flyer and baseplate properties. Waves do not form if the flyer is denser than the baseplate with a large density difference, or if the flyer has a much higher melting temperature. These results highlight the importance of material positioning and melting temperature, factors not considered by the previous equations. To account for this, the Wave Interface Factor (WIF) 2.8 was proposed, combining the density and melting temperature ratios of flyer to baseplate.

$$WIF = \frac{\rho_f}{\rho_b} \times \frac{T_{mf}}{T_{mb}} \tag{2.8}$$

ρ is the density and T_m is the melting temperature. The WIF predicts whether a wavy interface can form. Above a critical value, the interface remains flat regardless of welding parameters, below it, wave formation may occur depending on the parameters.

The equations reported in literature to define the left limit of the weldability window are summarised in Table 2.1.

Table 2.1 Equations reported in literature to define the left limit of the weldability window.

Equation	Formula	Author
2.1	$R_c = \frac{(\rho_f + \rho_b)V_c^2}{2(HV_f + HV_b)}$	Cowan et al. [30]
2.2	$KE = 93.02(\pm 9.62) - 13.45(\pm 2.06)\beta + 0.71(\pm)\beta^2 - 0.012(\pm 0.03)\beta^3$	Jaramillo et al. [32]
2.3	$KE = 175.53 - 15.995\beta + 0.5174\beta^2 - 0.0053\beta^3$	Vivek et al. [33]
2.6	$\Delta KE = 2V_C^2 h_f \rho_f (sin^2\beta/2)$	Salem et al. [35]
2.7	$\Delta KE = \rho_f V_C^2 \left(\frac{r_{fo}^2 - r_{fi}^2}{r_{bi}}\right) sin^2\frac{\beta}{2}$	Jirdehi et al. [25]
2.8	$WIF = \frac{\rho_f}{\rho_b} \times \frac{T_{mf}}{T_{mb}}$	Carvalho et al. [37]

2.2 Lower Limit

The weldability window's lower boundary is dictated by the need for sufficient impact pressure to induce jet formation at the collision point. This requires the metal to exhibit fluid-like behaviour, ensuring proper interfacial flow. The former condition is obtained when impact pressures greatly exceed the dynamic yield stress, which is largely influenced by the flyer plate velocity.

Through a comprehensive literature review, Lysak and Kuzmin [38] identified and organized the findings into three separate models - 1 - the hydrodynamic, 2 - energy approach and 3- pressure-time-temperature coordinates.

1. Wittman's [28] findings suggest that an effective estimation method involves multiplying the Hugoniot Elastic Limit (HEL) pressure by a factor of five and converting it into impact velocity using the pressure-particle velocity equation of state. When HEL data is unavailable, a reasonable approximation for determining the required impact conditions can be obtained using equation 2.9.

$$\beta = \sqrt{\frac{\sigma_b}{\rho V_c^2}} \tag{2.9}$$

σ_b is the ultimate tensile strength, although not specified for which plate.

Equation 2.9 is based mainly on the geometry of the plates. Building upon the work of Wittman [28], Deribas [39] further elaborated on the formula for defining the lower boundary and proposed relating the critical angle β to the Vickers Hardness H and, thus, extended the formula to consider both geometrical characteristics but also mechanical properties.

$$\beta = k\sqrt{\frac{HV}{\rho V_c^2}} \tag{2.10}$$

In Equation 2.10, k varies from 0.6 for plates with clean surfaces to 1.2 for imperfectly clean surfaces but with 1.14 being the most usual value for it. As ρ and HV, it was not specified by the authors if the parameters refered to the flyer or base plate. Shmorgun and Sonnov [40] later proposed the following relationship.

$$\beta = \frac{1}{\sqrt{1-(V_c^2/C_b^2)}}\sqrt{\frac{2\sigma_Y}{\rho V_c^2}} \tag{2.11}$$

This equation considers also the velocity of sound on the metal C_b and the yield stress σ_Y but it is also not mentioned by the authors to which plate the parameters refer to. Belayev et al. [41] attempted to relate the critical collision angle β with the tensile strength σ_b as follows.

$$\beta = 1.8\left[\frac{1}{V_c}\sqrt{\frac{\sigma_b}{\rho}} + 0.1\left(\frac{V_c}{C_b+1550}\right)^2\right] \tag{2.12}$$

Again, it is not mentioned by the authors to which plate the parameters refer to.

Lysak and Kuzmin [38] then plotted equations (2.9) to (2.12) as shown in Figure 2.10 and noted that the boundaries differ depending on the equation used and attributed those differences to the fact that the equations considered thus far do not account for the mass of the colliding plates.

2. Pursuing a better way of describing the lower boundary Shmorgun [42] introduced the average mass

$$\tilde{m} = \frac{\rho_f h_f \rho_b h_b}{\rho_f h_f + \rho_b h_b} \tag{2.13}$$

ρ_f, h_f, ρ_b and h_b are the the densities and thicknesses for the flyer and the base plate, respectively. Then, considering that energy used for the plastic deformation of the metal is located in an area with a width of twice the amplitude of the waves formed in the joint the authors obtained the following equation:

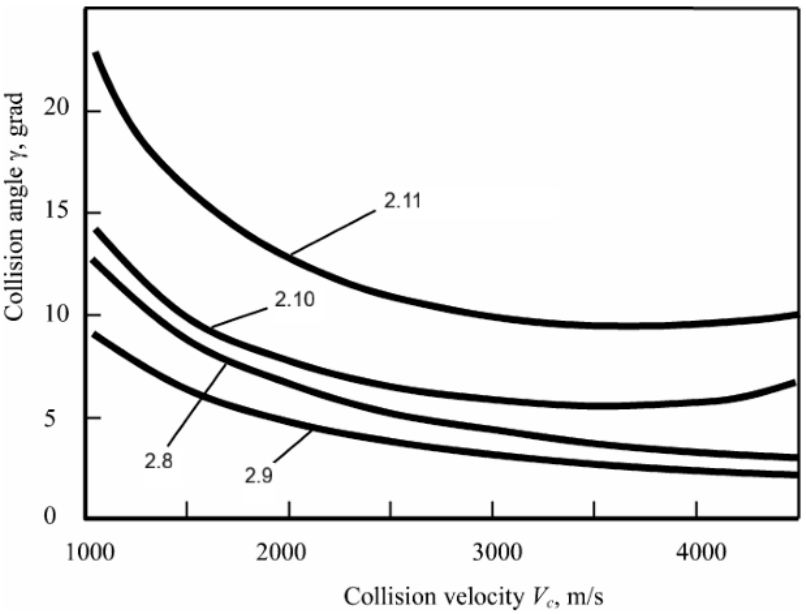

Figure 2.10 The lower boundary positions for explosive welding of low-carbon steel with low-carbon steel were calculated using various equations. Adapted from [38].

$$V_{i,cr} = \sqrt{\frac{\sigma_{0.2}}{2\rho(1-(V_c^2/C_b^2))}\left(1+\sqrt{1+\frac{4E_j}{\frac{\sigma_{0.2}h_f h_b}{(h_f+h_b)}}}\right)} \tag{2.14}$$

$V_{i,cr}$ is a critical value of the plate impact velocity, E_j is the energy necessary to join both plates, defined by:

$$E_j = 0.8 \times 2ac\rho T_m \tag{2.15}$$

$\sigma_{0.2}$ is the 0.2 % yield strength offset, a is the wave amplitude and c is the thermal capacity of the welded metals, however, it is not specified if they relate to the flyer or base plate.

Some concerns where however raised by Lysak and Kuzmin [38] to the above approach given that the chosen criteria of twice the amplitude was not substantiated by the authors and also, the fact that a good weld can occur without the presence of a wavy interface.

Nonetheless, the introduction of the average mass allowed Lysak and Kuzmin [38] to plot three dimensional limits seen in Figure 2.11 hence effectively advancing from a purely mechanistic approach to the energy approach. Any point of the space in the $\tilde{m} - \beta - V_c$ equates to a value of energy W_2 spent on metal deformation.

$$W_2 = V_i^2 \tilde{m}[1-(V_c/C_b)^2] \tag{2.16}$$

A good weld is then considered when the critical energy level W_2^{cr} is surpassed.

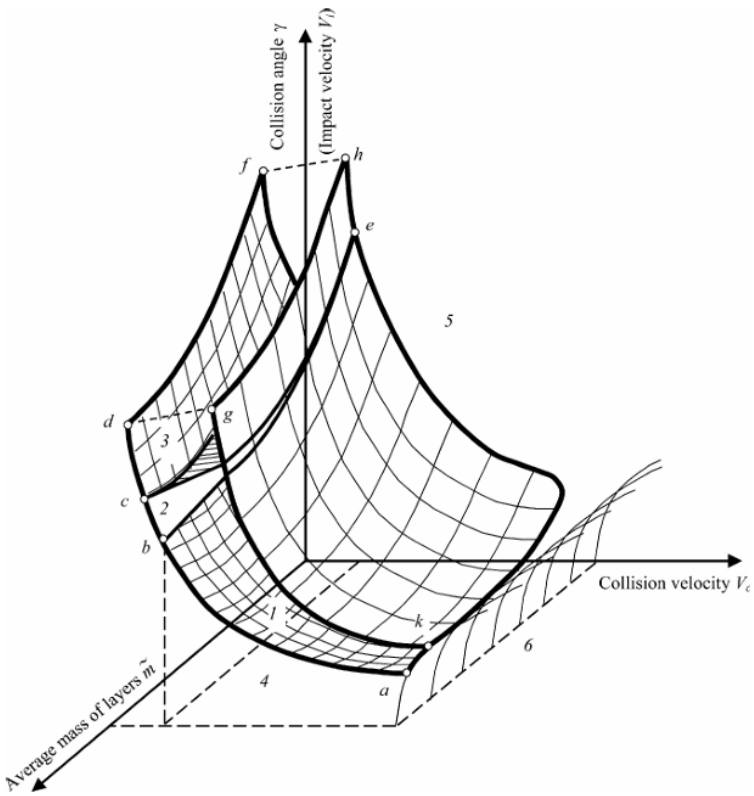

Figure 2.11 Three dimensional weldability window considering the average mass of the plates in the system. Position of basic characteristic areas of metal explosive welding: 1 – "traditional" regimes; 2 – waveless regimes; 3 – anomalous wave formation; 4 – pre-critical regimes; 5 – "out-of-limit" regimes; 6 – supersonic regimes.Adapted from [38].

3. Lysak et al. [43] introduced a new parameter I_d that refers to the pressure deforming pulse and was described by equation 2.17

$$I_d = \int_0^{\tau_w} p(\tau) d\tau = \int_0^{\tau_w} p_{max} e^{-\tau/\theta} d\tau \tag{2.17}$$

p_{max} is the maximum pressure felt in the collision point, τ_w is a time variable that defines the plastic deformation duration and θ is a time constant that describes the pressure gradient in the joint zone. With the introduction of time in the equation, the authors managed to achieve a lower boundary described by pressure, time and temperature. Equation 2.17 allows for the determination of the energy conditions of joint formation at pressure p.

By analysing multiple experimental data, both obtained by [43] and by other researchers, the authors managed to obtain a critical range of 3.5-3.7 kNs/m^2 (Figure 2.12) for the pressure deforming pulse I_d of low-carbon steels below which the quality of the joint decreases.

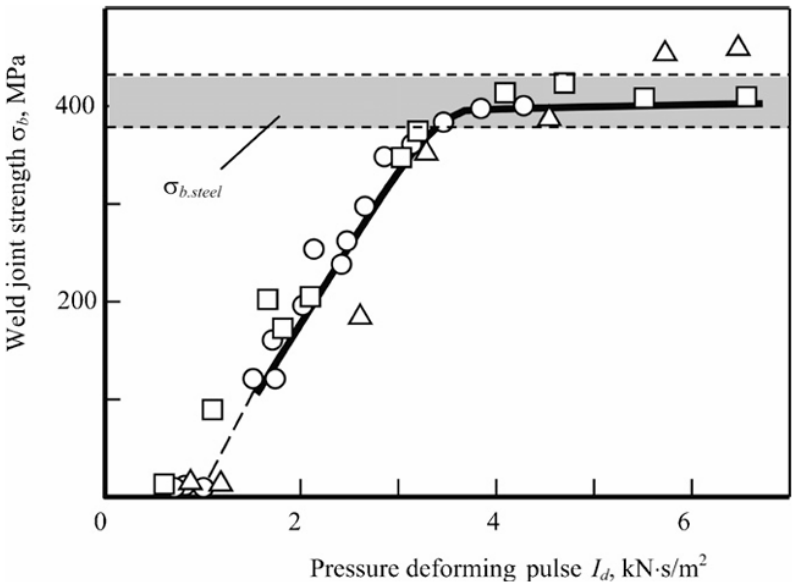

Figure 2.12 Influence of the pressure-deforming pulse I_d on the breaking strength σ_b of a low-carbon steel bimetal plate. Adapted from [38].

The equations reported in literature to define the lower limit of the weldability window are summarised in Table 2.2.

Table 2.2 Equations reported in literature to define the lower limit of the weldability window.

Equation	Formula	Author
2.9	$\beta = \sqrt{\frac{\sigma_b}{\rho V_c^2}}$	Wittman et al. [28]
2.10	$\beta = k\sqrt{\frac{HV}{\rho V_c^2}}$	Deribas et al. [39]
2.11	$\beta = \frac{1}{\sqrt{1-(V_c^2/C_b^2)}}\sqrt{\frac{2\sigma_Y}{\rho V_c^2}}$	Shmorgun et al. [40]
2.12	$\beta = 1.8\left[\frac{1}{V_c}\sqrt{\frac{\sigma_b}{\rho}} + 0.1\left(\frac{V_c}{C_b+1550}\right)^2\right]$	Belayev et al. [41]
2.14	$V_{i,cr} = \sqrt{\frac{\sigma_{0.2}}{2\rho(1-(V_c^2/C_b^2))}\left(1+\sqrt{1+\frac{4E_j}{\frac{\sigma_{0.2}h_f h_b}{(h_f+h_b)}}}\right)}$	Shmorgun et al. [42]
2.17	$I_d = \int_0^{\tau_w} p(\tau)d\tau = \int_0^{\tau_w} p_{max}e^{-\tau/\theta}d\tau$	Lysak et al. [43]

2.3 Upper Limit

The upper boundary in explosive welding represents the maximum impact velocity that prevents excessive melting at the interface, dictated by the collision velocity, material properties, and melting temperature. As the collision angle and velocity increase, more heat is generated, with kinetic energy from impact converting into heat through deformation and friction. If cooling is insufficient, melting occurs, leading to intermetallic compounds and defects [10, 27, 29].

Carpenter and Wittman [10] were able to derive equation 2.18 for the maximum flyer plate velocity:

$$sin\frac{\beta}{2} = \frac{1}{N}\frac{\sqrt{T_m C_b}}{2V_c^2}\frac{\sqrt[4]{KC_pC_b}}{\rho h_f} \tag{2.18}$$

N is a constant which differs for different metals and can be calculated for each or an average value of 0.11 can be considered [44].

According to Zhou et al. [45], Deribas [46] also formulated an equation 2.19 to represent this phenomenon as follows:

$$sin\frac{\beta}{2} = \sqrt{\frac{E}{3\rho(1-2\nu)}} \times \frac{1}{2h^{0.25}V_c^{1.25}} \tag{2.19}$$

However, Yang et al. [47] in their work used equation 2.20 also obtained by Deribas [46] which is only slightly different, however, the altered formula was introduced without justification from data or theory.

$$sin\frac{\beta}{2} = \sqrt{\frac{E}{6\rho(1-2\nu)}} \times \frac{1}{h^{0.25}V_c^{1.25}} \tag{2.20}$$

ν is the Poisson Coefficient and E is the Young's Modulus.

Wang et al. [48] in their work on explosive welding for nuclear fusion equipment used the equation 2.21 to define the upper limit:

$$V_p = \frac{f}{V_c}\sqrt{1+\frac{\rho_b h_b}{\rho_f h_f}}\sqrt[4]{Min\left(1, \frac{h_f C_{b_b}}{h_b C_{b_f}}\right) \Big/ h_b} \tag{2.21}$$

Equation 2.21 can also be expressed by β using Equation 2.22 as follows.

$$V_p = 2 \times V_c \times sin\frac{\beta}{2} \tag{2.22}$$

$$sin\frac{\beta}{2} = \frac{f}{2V_c^2}\sqrt{1+\frac{\rho_b h_b}{\rho_f h_f}}\sqrt[4]{Min\left(1, \frac{h_f C_b}{h_b C_f}\right) \Big/ h_b} \tag{2.23}$$

f is the experimental coefficient, which is a constant whose value must be experimentally obtained, related to the physical properties of the metal but no procedure to obtain or calculate it was specified. Additionally, no background on the development of the equation was available.

Efremov and Zhakarenko [49] developed a new approach to determine the upper limit on explosive welding for identical materials, noting that similar formulas could possibly be obtained for dissimilar materials but that additional research on that subject would be required. To determine the upper limit, the authors explain that the solidification time t_2 at the interface should be less than the time t_1 for which the positive pressure persists at the joint in order to produce a sound welded joint.

$$t_2 \leq t_1 \tag{2.24}$$

t_2 can be obtained as follows:

$$t_2 = \frac{1.6 \times 10^{-4} V_c^4 \rho^2 h_f^2 sin^4(\beta/2)}{\pi T_m^2 (\frac{K}{\alpha})^2} \times \left(\frac{h^2}{h_f + h_b}\right)^2 \tag{2.25}$$

K is the Thermal Conductivity and α is the Thermal Diffusivity. There is no indication of which plate material Tm, ρ, α and K to use in case of using different materials for the flyer and base plate. t_1 can be obtained as follows:

$$t_1 = \xi h_f / v_c \tag{2.26}$$

ξ can be calculated as follows or be considered equal to 1.

$$\xi = 0.5 + 0.66 \frac{\rho V_c^2}{G} \tag{2.27}$$

G is the shear modulus, again, with no mention of which plate it refers to. Kuz'min et al. [50] studied the critical conditions of the formation and failure of welded joints in explosive welding and, similarly to Efremov and Zakharenko [49] expressed the upper boundary of the weldability window starting from a comparison between the time it takes the unloading waves to arrive to the welding zone, t_p and the solidification time t_s. The authors reported that the strongest effect of these waves was observed when the molten areas of the interface have not yet fully solidified, possibly leading to complete failure of the joint. Thus, to achieve a sound joint t_p should be inferior to t_s.

$$t_p \leq t_s \tag{2.28}$$

$$t_p = 0.5 + 0.66(\rho_f V_c^2 / G) \frac{h_f}{V_c} \tag{2.29}$$

where G is the shear modulus of the metal.

$$t_s = \frac{1.15 \times 10^{-3} \rho_f V_c^4 h_f^2 \left(\frac{h_b}{h_f + h_b}\right)^2 sin^4 \frac{\beta}{2}}{\pi C_p K T_m^2} \tag{2.30}$$

The equations reported in literature to define the upper limit of the weldability window are summarised in Table 2.3.

Table 2.3 Equations reported in literature to define the upper limit of the weldability window.

Equation	Formula	Author
2.18	$sin\frac{\beta}{2} = \frac{1}{N}\frac{\sqrt{T_m C_b}}{2V_c^2}\frac{\sqrt[4]{kC_pC_b}}{\rho h}$	Carpenter et al. [10]
2.19	$sin\frac{\beta}{2} = \sqrt{\frac{E}{3\rho(1-2\nu)}} \times \frac{1}{2h^{0.25}V_c^{1.25}}$	Ma et al. [45]
2.20	$sin\frac{\beta}{2} = \sqrt{\frac{E}{6\rho(1-2\nu)}} \times \frac{1}{h^{0.25}V_c^{1.25}}$	Yang et al. [47]
2.23	$sin\frac{\beta}{2} = \frac{f}{2V_c^2}\sqrt{1+\frac{\rho_b h_b}{\rho_f h_f}}\sqrt[4]{Min\left(1, \frac{h_f C_{b_b}}{h_b C_{b_f}}\right)\Big/ h_b}$	Wang et al. [48]
2.24	$t_2 \leq t_1$	Zhakarenko et al. [49]
2.25	$t_2 = \frac{1.6\times10^{-4}V_c^4\rho^2h_f^2sin^4(\beta/2)}{\pi T_m^2(\frac{K}{\alpha})^2} \times \left(\frac{h^2}{h_f+h_b}\right)^2$	Zhakarenko et al. [49]
2.26	$t_1 = \xi h_f / V_c$	Zhakarenko et al. [49]
2.28	$t_p \leq t_s$	Kuzmin et al. [50]
2.29	$t_p = 0.5 + 0.66(\rho_f V_c^2/G)\frac{h_f}{V_c}$	Kuzmin et al. [50]
2.30	$t_s = \frac{1.15\times10^{-3}\rho_f V_c^4 h_f^2\left(\frac{h_b}{h_f+h_b}\right)^2 sin^4\frac{\beta}{2}}{\pi C_p K T_m^2}$	Kuzmin et al. [50]

2.4 Right Limit

The right limit on the weldability window represents the transition from jet occurring conditions to non-jet occurring conditions where a jet is considered a high-speed stream of material. Ideally, in explosive welding, a high-velocity jet forms when two mating surfaces collide at a velocity and angle that exceed critical thresholds necessary for bonding. The oxide films typically present on metal surfaces act as a barrier to achieving a true metallurgical bond. However, the forward-moving jet plays a crucial role in removing these oxide layers, thereby cleaning the surfaces and making them suitable for bonding [30, 51].

Walsh et al. [52] studied what happened when two solid objects collided at very high speeds, especially focusing on when a jet is formed at the collision point. The authors proposed two types of collisions - Jetless collisions and Jet-forming collisions. They developed a theory based on fluid dynamics principles, assuming that under very high pressures, solid materials behave like compressible fluids. A key result was that whether a collision produces a jet depends critically on the collision angle and the velocity of the materials. If the collision angle is below a certain critical value, a jet will not form. If the angle is above this critical value, a jet will form. Experiments were conducted by colliding metal plates accelerated by explosives. The collisions were recorded using high-speed cameras. The experimental results were compared with theoretical predictions:

- Jetless collisions were observed when the collision angle was below the predicted critical angle.
- Jet formation occurred at angles above the critical value.
- The experimental results generally matched the theory well.

The experimental results generally matched the theory well and the overall conclusion was that the theory accurately predicts when jet formation occurs, validating the proposed model. The results also provided indirect support for certain equations describing how materials behave under extreme pressures.

Following on the work of Walsh, Cowan and Holtzman [53] investigated the flow dynamics and bonding mechanisms involved in EXW. The study corrects and extends earlier theoretical models, especially in defining the conditions that govern jetting in asymmetric collisions. As mentioned, a jet is produced when the plates collide under specific combinations of collision angle and collision velocity. The study distinguishes between subsonic and supersonic collision regimes. In the subsonic regime, where the relative velocity between the plates is less than the speed of sound in the materials, jet formation can occur over a relatively wide range of conditions. Here, the physics is governed by compressible but continuous flow, and no attached shock waves are expected. In this regime, jetting occurs more reliably as long as the collision angle is not too small, allowing the interface materials to undergo sufficient shear and plastic deformation. The subsonic regime is particularly favourable for ductile materials and combinations with relatively similar densities and sound speeds, which help maintain stable flow during the jetting process. The study shows that in this regime, jet formation does not require a critical angle in the strict sense, but there is still a practical lower bound to the collision angle, if it is too shallow, the interface may only slide or compress without sufficient jetting energy, resulting in weak or no bonding. For the supersonic regime, where the collision velocity exceeds the speed of sound in at least one of the materials, attached oblique shock waves can form at the interface. These shocks can suppress jet formation unless the collision angle is steep enough to force shock detachment, at which point jetting becomes possible. This leads to the definition of a critical collision angle that depends on material properties and impact speed.

Below this critical angle, the collision remains jetless, and no bond is formed. Thus, the the sonic velocity of the flyer plate can be used to define the right boundary as follows

$$V_c < C_b \tag{2.31}$$

Several authors [26, 54, 55] also report that Abrahamson [56] defined the limiting curve for the jet formation as

$$V_c = \frac{\beta}{10} + 5.5 \tag{2.32}$$

The equations reported in literature to define the right limit of the weldability window are summarised in Table 2.4.

Table 2.4 Equations reported in literature to define the right limit of the weldability window.

Equation	**Formula**	**Author**
2.31	$V_c < C_b$	Walsh et al. [52]
2.32	$V_c = \frac{\beta}{10} + 5.5$	Abrahamson et al. [56]

Chapter 3

Results and Discussion

In this chapter an analysis of experimental data obtained from the literature is performed. With the goal of obtaining a rough predictor of weld quality, the data is analysed from the collision velocity and kinetic energy perspective. Then, the equations from Chapter 2 are revisited one by one and analysed, a comparison of theoretical results versus experimental results is made where possible and the limitations found are described for each. Only welds consisting of just base and flyer plates were considered.

3.1 Kinetic Energy

Experimental data was gathered from Carvalho et al. previous work [37, 57–65] and Galvão et al. [66] in order to compare the experimental results to the theoretical results obtained by using the formulas from Chapter 2. The data is organised in Table 3.1. It is worth noting that for all weld series only the collision point velocity was experimentally obtained and the flyer plate impact velocity and the collision angle were calculated using Equations 2.22 and 3.1. Additionally, for all series considered the configuration was parallel without the use of interlayers.

$$V_p = \sqrt{2E}\left(\frac{3R^2}{R^2+5R+4}\right)^{1/2} \tag{3.1}$$

$\sqrt{2E}$ represents the Gurney characteristic velocity and R the explosive ratio. This can also introduce error on the results that follow.

Where individual property values were not reported by the original sources, standard values were taken from the AZoM materials database for the corresponding material [67]. All material properties are summarised in Table 3.2. The use of standard property values may introduce some error to the analysis and when performing experiments the values should, ideally, be experimentally obtained for all materials.

Table 3.1 Experimental data gathered from Carvalho et al. previous work [37, 57–65] and Galvão et al. [66].

#	Ref.	Base	h_b [mm]	HV	ρ [g/cm^3]	Flyer	h_f [mm]	HV	ρ [g/cm^3]	V_c [m/s]	V_p [m/s]	B [º]	Success?
1	[56]	Cu-DHP	3	94	8.96	AISI 304	3	188	8	2186	446	11.77	Y
2	[56]	AISI 304	3	188	8	Cu-DHP	3	94	8.96	2420	403	9.59	Y
3	[57]	AISI 304	3	181	8	AA6082-T6	3	114	2.7	2300	703	17.80	Y
4	[57]	AISI 304	3	181	8	AA6082-T6	3	114	2.7	2836	523	10.63	N
5	[57]	EN DC06	3	99	7.85	AA6082-T6	3	114	2.7	1938	592	17.79	Y
6	[57]	EN DC06	3	99	7.85	AA6082-T6	3	114	2.7	2836	523	10.63	Y
7	[58]	AA6082-T6	3	114	2.7	Cu-DHP	1	94	8.96	2121	642	17.62	Y
8	[60]	AA6082-T6	3	114	2.7	AA6082-T6	3	114	2.7	3523	1051	17.36	Y
9	[60]	AA6082-T6	3	114	2.7	AA6082-O	3	42	2.7	3477	1037	17.35	Y
10	[60]	AA6082-T6	3	114	2.7	Cu-DHP	1	94	8.96	3430	973	16.48	Y
11	[61]	Cu-DHP	3	94	8.96	Cu-DHP	1	94	8.96	3551	1013	16.58	Y
12	[61]	Cu-DHP	3	94	8.96	AA6082-T6	3	114	2.7	3589	1072	17.38	N
13	[61]	Cu-DHP	3	94	8.96	AA6082-T6	3	114	2.7	2077	577	16.13	Y
14	[62]	AA6082-T6	15	111	2.7	EN DC06	3	116	7.86	3172	372	6.73	N
15	[62]	AA6082-T6	15	111	2.7	EN DC06	3	116	7.86	3514	497	8.13	N
16	[62]	AA6082-T6	15	111	2.7	EN DC06	3	116	7.86	2300	404	10.12	Y
17	[62]	AA6082-T6	15	111	2.7	EN DC06	3	116	7.86	2072	296	8.21	N
18	[63]	AA6082-T6	15	111	2.7	AISI 304	3	181	8	3514	481	7.87	N
19	[63]	AA6082-T6	15	111	2.7	AISI 304	3	181	8	3527	671	10.97	N
20	[63]	AA6082-T6	15	111	2.7	AISI 304	3	181	8	3172	367	6.64	N
21	[63]	AA6082-T6	15	111	2.7	AISI 304	3	181	8	2300	393	9.84	N
22	[63]	AA6082-T6	15	111	2.7	AISI 304	3	181	8	2537	462	10.49	N
23	[63]	AISI 304	3	180	8	AA6082-T6	3	114	2.7	2300	697	17.64	Y
24	[63]	AISI 304	3	180	8	AA6082-T6	3	114	2.7	2077	559	15.61	Y
25	[66]	AA5083	30	84	2.65	Cu-DHP	3	94	8.96	1647	210	7.33	Y
26	[66]	AA5083	30	84	2.65	Cu-DHP	3	94	8.96	2072	350	9.72	Y
27	[66]	AA5083	30	84	2.65	Cu-DHP	1	94	8.96	1712	383	12.93	Y
28	[66]	AA5083	30	84	2.65	Cu-DHP	1	94	8.96	1855	481	15.03	Y
29	[66]	AA5083	30	84	2.65	Cu-DHP	1	94	8.96	2013	586	16.92	Y
30	[66]	AA5083	30	84	2.65	Cu-DHP	1	94	8.96	2149	673	18.25	Y
31	[66]	AA6082-T6	3	114	2.7	Cu-DHP	1	94	8.96	2121	704	19.39	Y
32	[66]	AA6082-T6	3	114	2.7	Cu-DHP	1	94	8.96	2271	859	22.23	Y
33	[66]	AA6082-T6	3	114	2.7	Cu-DHP	1	94	8.96	3275	817	14.45	Y
34	[66]	AA6082-T6	3	114	2.7	Cu-DHP	1	94	8.96	3430	974	16.50	Y
35	[66]	Cu-DHP	3	94	8.96	AA6082-T6	3	114	2.7	2077	577	16.13	Y
36	[66]	Cu-DHP	3	94	8.96	AA6082-T6	3	114	2.7	2987	947	18.48	N
37	[66]	Cu-DHP	3	94	8.96	AA6082-T6	3	114	2.7	3256	596	10.55	N
38	[66]	Cu-DHP	3	94	8.96	AA6082-T6	3	114	2.7	3256	726	12.88	N
39	[66]	Cu-DHP	3	94	8.96	AA6082-T6	3	114	2.7	3477	1037	17.35	N
40	[66]	Cu-DHP	3	94	8.96	AA6082-T6	3	114	2.7	3589	1072	17.38	N
41	[66]	Cu-DHP	3	94	8.96	AA6082-T6	3	114	2.7	3665	823	12.98	N
42	[66]	Cu-DHP	3	94	8.96	AA6082-T6	5	114	2.7	2077	435	12.09	Y

Table 3.2 Material properties for the plates analysed [67].

	AISI 304	Cu-DHP	AA6082-T6	AA6082-O	EN DC06	AA6082	AA5083
C_b [m/s]	5920	4660	6320	6320	5890	6320	6350
σ_y [MPa]	220	125	270	72.5	145	170	177.5
σ_b [MPa]	620	280	325	130	300	225	327.5
Tm [ºC]	1400	1084	650	600	1490	600	605
K [W/(m·ºC)]	16	330	180	180	50	180	121
Cp [J/(kg·ºC)]	500	385	900	900	485	900	900
E [GPa]	193	110	70	70	210	70	70
ν	0.29	0.34	0.33	0.33	0.30	0.33	0.33
α [m^2/s]	4.00E-06	9.59E-05	7.41E-05	7.41E-05	1.31E-05	7.41E-05	5.07E-05
G [GPa]	77	44	26	26	80	26	26

The first step was to calculate the kinetic energy which was obtained as follows

$$KE_f = \frac{1}{2} \times \rho_f \times h_f \times Vp^2 \tag{3.2}$$

where KE is the kinetic energy [kJ/m^2], ρ is the density [kg/m^3], V_p the velocity in [m/s] and hf is the thickness of the flyer plate [m]. The results can be seen in Figure 3.1. For all plots the XX axis represents the collision point velocity and the YY axis represents the KE. In Figure 3.1 all datasets were plotted and it is possible to assess that the higher the velocity and the kinetic energy, the less likely it is to have a successful weld. A full study of welding success should be performed for pairs of materials as well for a complete understanding of how different metal combinations affect the results of explosive welding. However, due to not enough data for each pair of materials and considering the fact that flyer plate characteristics play a major role in defining the weldability window [68], a study was conducted considering only the flyer plate material. Thus, the experimental data was divided by flyer plate material - Aluminium, Copper, Stainless Steel and Carbon Steel.

Figure 3.1b plots the results for all experiments using an aluminium flyer. Although there is an outlier where a successful weld was obtained at high velocity the same behaviour as before can be seen where the higher the velocity and kinetic energy, the less likely it is for the weld to be successful. Furthermore, it is also possible to observe that the collision point velocity is a better predictor of the weld quality as above around 2600 m/s only one weld was successful, which was not expected and is considered an outlier. However, there is no value for the kinetic energy that establishes a hard separation between the unsuccessful and the successful welds.

Figure 3.1c plots the results for all experiments using a copper flyer. In this case, the copper's ability to create a successful weld seems to be less affected by the high kinetic energy and velocity. This behaviour could possibly be due to copper's high thermal conductivity and medium high melting temperature allow it to dissipate heat efficiently during impact, preventing local melting and formation of intermetallic compounds even at elevated collision velocities and/or due to its high ductility and relatively high density allow the material to absorb the collision energy without cracking and to generate sufficient interfacial pressure for effective cleaning and bonding

Figures 3.1d and 3.1e plot the results for experiments using carbon steel and stainless steel, respectively, and the same analyses from Figure 3.1b can be applied here, however, for Figure 3.1d the velocity threshold isn't as hardly defined and could be anywhere between 2400 and 3100 m/s whereas for Figure 3.1e the velocity threshold is set at around 2250 m/s. These velocities should only be considered as approximations and a more detailed study with more data should be conducted to obtain more precise results, as aforementioned.

3.2 Weldability Limits Analysis

With the relationship between kinetic energy, collision velocity and weld quality established, the following sections focus on the analysis of the individual limits that define the weldability window. The subsequent discussion revisits the theoretical formulations presented in Chapter 2 and compares them with the experimental results in order to evaluate their accuracy and applicability to the studied material pairs.

3.2.1 Left Limit

Equation 2.1 was calculated using all SI units and the results were compared to a value of $R_c = 10.6$ as defined by Cowan et al. [30]. If the equation returned Rc over 10.6 a wavy interface should be expected and under 10.6 a waveless interface should be expected. The results can be seen in Figure 3.2 where the blue colour represents a data point which experimental and theoretical results are in agreement and the orange colour represents that these are in disagreement. If comparing wavy predictions to successful welds and waveless predictions to unsuccessful welds, the equation had a prediction rate of 50 %. However, as pointed out before a wavy interface is not fundamentally necessary nor a indicator of a successful weld and it is possible to have a successful weld with a waveless interface as long as the interface is clean of impurities. Therefore, to have a better understanding of how good of a predictor this equation is, information on the characteristics of the interface should be available and used for comparison instead. The same will apply for Equations 2.2 and 2.3.

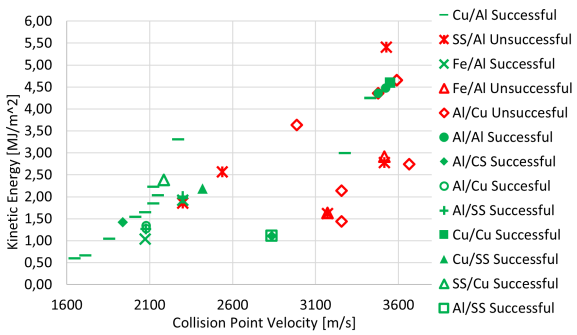

(a) Plot of Kinetic Energy versus Collision Point Velocity for all weld series.

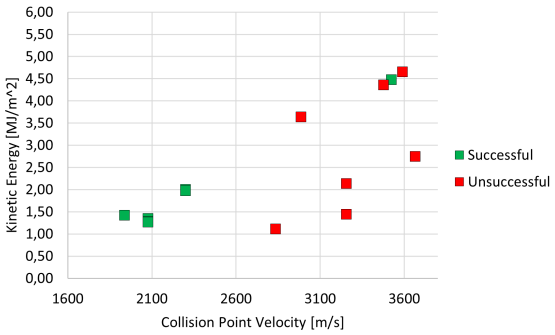

(b) Plot of Kinetic Energy versus Collision Point Velocity for all welds using a All flyer plate.

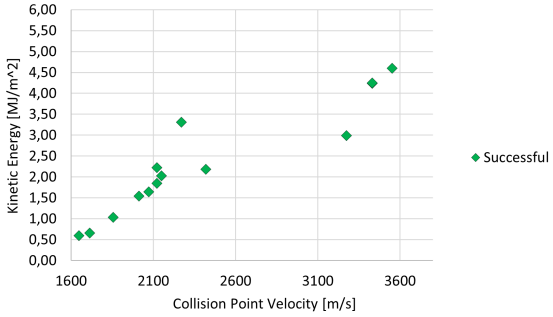

(c) Plot of Kinetic Energy versus Collision Point Velocity for all welds using a Cu flyer plate.

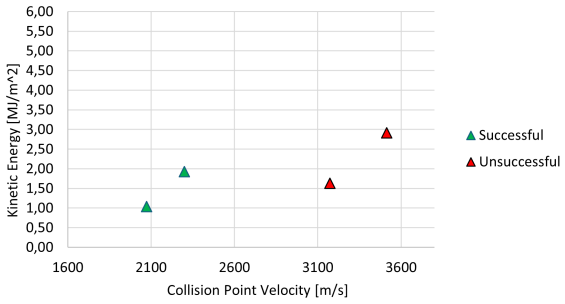

(d) Plot of Kinetic Energy versus Collision Point Velocity for all welds using a CS flyer plate.

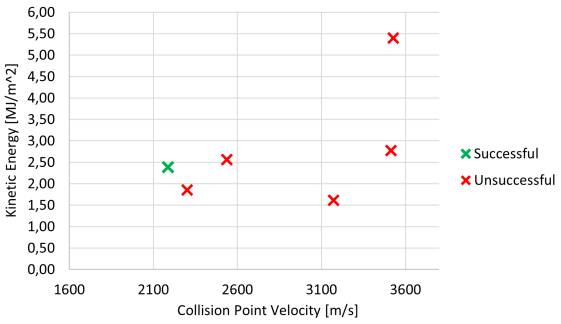

(e) Plot of Kinetic Energy versus Collision Point Velocity for all welds using a SS flyer plate.

Figure 3.1 Kinetic energy vs Collision Point Velocity analysis plots.

With the above note in mind, Equation 2.2 was analysed. As per Jaramillo et al. [32] the critical value of R_c which he mentioned was the same as KE was calculated using his equation and this was considered the critical value which would then be compared with the value of R_c as per Equation 2.1 as done above. This way, instead of assuming a constant threshold value for every β, the critical value will depend on β as well. The results are illustrated in Figure 3.3. Again, if comparing wavy predictions to successful welds and waveless predictions to unsuccessful welds, the equation had a prediction rate of 57 % which is an improvement over Equation 2.1.

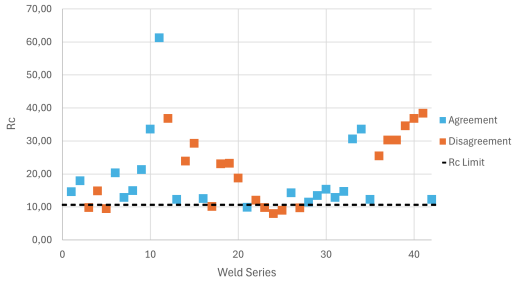

Figure 3.2 Plot of Rc versus Weld series highlighting results for Equation 2.1.

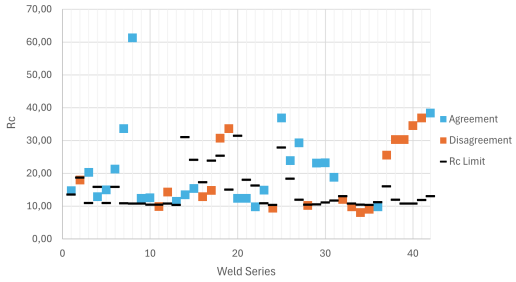

Figure 3.3 Plot of Rc versus Weld series highlighting results for Equation 2.2.

The same procedure was performed for Equation 2.3 and the results can be seen in Figure 3.4. This time the equation only had a prediction rate of 36 %. This discrepancy can be explained by the fact that both Equations 2.2 and 2.3 were obtained experimentally and, thus, will be biased towards the pair of materials used and the characteristics and properties of the plates. An attempt could be made in the future to perform multiple welds with varying materials and plate characteristics in order to obtain an universal equation or obtain multiple approximate equations for each pair of materials.

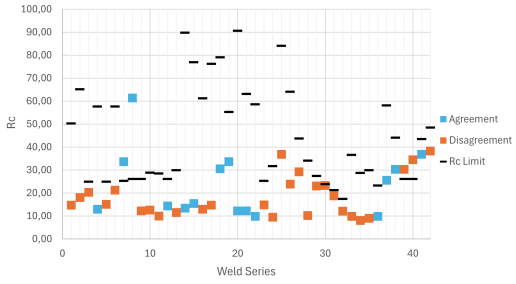

Figure 3.4 Plot of Rc versus Weld series highlighting results for Equation 2.3.

For equation 2.7, as described before, the authors experimentally obtained a critical kinetic energy value below which the wavelength would go to infinity and, thus, the interface would be waveless instead of wavy. This critical value couldn't be tested in this work as no cylindrical explosive welding data was available.

Finally, equation 2.3 was also not tested against experimental data. This equation provides the loss of kinetic energy during collision and, therefore, could potentially be used as a generalisation of equation 2.7 for parallel configurations. Still, a critical value of kinetic energy should be obtained experimentally by comparing the wavelength to the kinetic energy as was done by Jirdehi et al. [25]. Hence, the equation was not tested in this work and, instead, is open for future analysis.

3.2.2 Lower Limit

The procedure follow for Equations 2.9, 2.10, 2.11 and 2.12 was identically as they are all already expressed in terms of β. Using all SI units the equations were used to calculate the critical value of β and the experimental values of β were compared against the critical value. If β is a higher value than the critical value, a successful weld is expected. It is worth noting that where the variables weren't explicitly defined if they referred to the flyer or base plate, they were considered for the flyer plate in accordance with Elango et al. [68] claims. The results are plotted in Figures 3.5, 3.6, 3.7 and 3.8 and the rates of predictability are 60 %, 53 %, 65 % and 55 %, respectively.

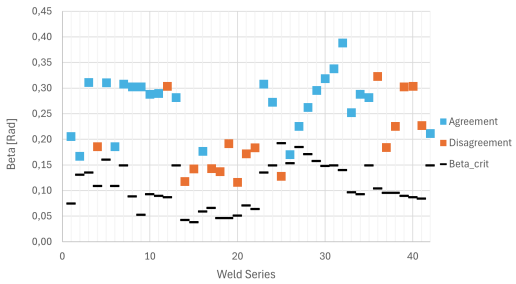

Figure 3.5 Plot of β_{cr} versus Weld series highlighting results for Equation 2.9.

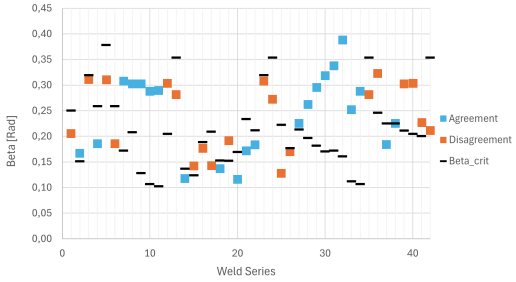

Figure 3.6 Plot of β_{cr} versus Weld series highlighting results for Equation 2.10.

As before, the dash symbolises the critical value for each weld series and for the data point, the blue colour represents an agreement between experimental and theoretical results and orange represents a disagreement.

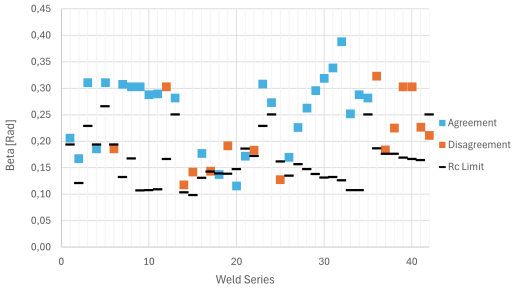

Figure 3.7 Plot of β_{cr} versus Weld series highlighting results for Equation 2.11.

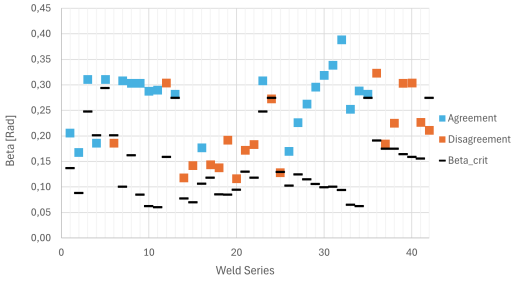

Figure 3.8 Plot of β_{cr} versus Weld series highlighting results for Equation 2.12.

It is noticeable that the squares maintain their position in all plots as the experimental value of β doesn't change, only the critical value obtain by the equations.

Equations 2.14 and 2.17 couldn't be analysed due to lack of data. For the first one, the calculation of the parameter E_j by Equation 2.15 requires the wave amplitude which isn't readily available and for the latter τ_w and θ which are also not available. Thus, these two equations remain open for future analysis.

3.2.3 Upper Limit

Concerning the upper boundary, Equations 2.18, 2.19 and 2.20 were calculated in regards to β to obtain the critical value but, this time, the value of β_{cr} is the upper cap and a successful weld should be expected theoretically for values below the critical one. All SI units were considered as well for the three equations, however, for Equations 2.18 and 2.19 some results returned a mathematical error as the argument for the arcsin would in those cases be higher than 1, and arcsin arguments range from negative 1 to positive one, returning negative $\pi/2$ to positive $\pi/2$. In such cases, the maximum value was considered. The equations has a prediction rate of 65 %, 62 % and 62 % and the results are plotted in Figures 3.9, 3.10 and 3.11.

Even though the prediction rates are high, by looking at the plots it is observable how far apart the critical values are from the experimental ones. For Equations 2.19 and 2.20 this is even more noticeable and should be pointed out that even though 15 welds of the total welds were unsuccessful, for both equations no data point is near or over the critical value, hence, this equations should be further refined.

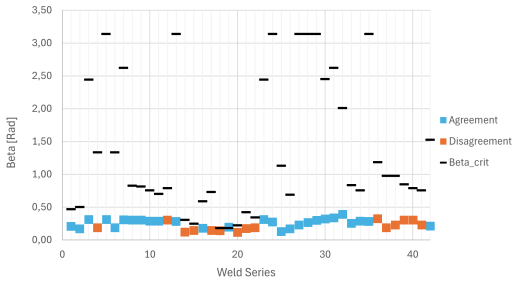

Figure 3.9 Plot of β_{cr} versus Weld series highlighting results for Equation 2.18.

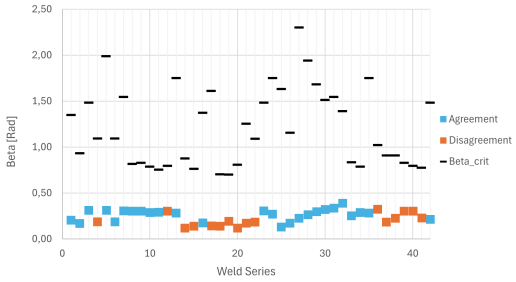

Figure 3.10 Plot of β_{cr} versus Weld series highlighting results for Equation 2.19.

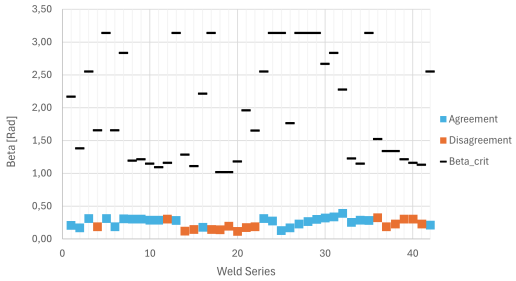

Figure 3.11 Plot of β_{cr} versus Weld series highlighting results for Equation 2.20.

Equation 2.23 couldn't be analysed as the coefficient f is to be obtained experimentally. This Equation remains open for future work.

In regards to Equations 2.24, 2.25 and 2.26, Equation 2.26 was successfully used considering $\xi = 1$. However, Equation 2.25 returned t_2 considerably distant from t_1, about 9 orders of magnitude smaller. Thus, these equations didn't return any valid results and a careful review of the two formulas is warranted as a possible transcription mistake could explain the discrepancy.

3.2.4 Right Limit

Equation 2.31 was used with SI units for both the collision point velocity and the bulk sound velocity. Both velocities were compared and the collision point velocity was inferior to the bulk sound velocity for all datasets considered and thus, indicates theoretical jet formation for all.

As for Equation 2.32, the units used weren't SI units but instead β in radians and V_c in

mm/μs in accordance with Ribeiro et al. [26]. Using β in radians makes the formula return a V_c which is nearly constant. As expected, when compared against the experimental V_c, all datasets theoretically should have jetting occur.

In the datasets used, the original sources did not report whether jetting occurred. As a result, the analysis indicates only that the tested points lie to the left of the calculated boundary and cannot confirm the presence or absence of jetting at those conditions. This lack of observation limits validation: agreement or disagreement relative to a jetting threshold cannot be assessed, a data-based onset of jetting cannot be defined, and empirical constants cannot be calibrated against such a threshold. In practical applications, this boundary is not typically the controlling constraint; EXW is usually operated at collision point velocities well below this level [69].

Given the missing jetting information, the right-hand limit is treated here as an upper cap inferred from Equations 2.31 and 2.32 rather than a boundary anchored to verified jetting events. Future work should draw on datasets that explicitly document jetting (e.g., by high-speed imaging) and report the essential conditions (collision point velocity and angle, stand-off, thicknesses, and relevant sound speeds). With such data, this boundary can be verified and, if necessary, refined to improve the predictive use of the weldability window for EXW.

Chapter 4

Conclusion

This study examined how well the weldability window predicts outcomes in explosive welding. The usual equations for the four boundaries were revisited. Where data allowed, their predictions were compared with reported results, and the main limitations and weak points of each equation were noted. The aim was not to build a full model but to clarify what the current framework can and cannot do.

The results show that collision velocity can be a useful first indication of weld quality, but its value depends on the flyer plate material and characteristics. For the left and lower boundaries, agreement with reported results was mixed across materials and test conditions. For the upper boundary, calculated limits often did not match the experimental ranges and were sensitive to input properties, which suggests that this boundary needs further work. For the right-hand boundary, the calculated limits lay to the right of all operating points in the datasets used; however, the sources did not state whether jetting occurred, so that boundary could not be checked directly. Overall, the weldability window acts as a practical qualitative guide rather than a consistent quantitative predictor across systems.

Two issues limit the conclusions: many papers do not report key inputs (such as measured thermal properties, stand-off and thickness effects), and most do not provide direct evidence of jetting or presence of waves in the interface. Future work should prioritise better reporting of inputs and outcomes, targeted tests that include conditions near the upper and right-hand boundaries, and systematic studies of how flyer/base placement and thickness influence the result. It should also examine the use of interlayers and how they shift the window, with a consistent way to record interlayer properties and geometry. Collecting such data across a representative set of material pairs and geometries would allow calibration and, where needed, revision of the boundaries, improving the accuracy and practical use of the weldability window in process design.

References

[1] R. W. Messler, *Principles of Welding*, ch. 1, pp. 3–5. John Wiley Sons, Ltd, 1999.

[2] R. W. Messler, *Principles of Welding*, ch. 2, pp. 23–25. John Wiley Sons, Ltd, 1999.

[3] W. Cai, G. Daehn, A. Vivek, J. Li, H. Ali, R. Mishra, and M. Komarasamy, "A state-of-the-art review on solid-state metal joining," *Journal of Manufacturing Science and Engineering*, 06 2018.

[4] B. Crossland, *Explosive Welding of Metals and Its Application*, ch. 1, pp. 1–3. Oxford science publications, Clarendon Press, 1982.

[5] H. E.-S. T.Z. Blazyski, *Explosive Welding, Forming and Compaction*, ch. 6. Applied Science Publishers London and New York, 1983.

[6] R. W. Messler, *Principles of Welding*. John Wiley Sons, Ltd, 1999.

[7] A. Loureiro, G. H. Carvalho, I. Galvão, R. M. Leal, and R. Mendes, *Explosive welding*, pp. 207–237. Elsevier, 1 2020.

[8] B. B. Sherpa, M. Kuroda, T. Ikeda, K. Kawamura, D. Inao, S. Tanaka, and K. Hokamoto, "Investigation of interfacial microstructure and mechanical characteristics of ti/ss316 clads fabricated by explosive welding process," *International Journal of Advanced Manufacturing Technology*, vol. 128, pp. 1403–1418, 9 2023.

[9] B. Crossland, *Explosive Welding of Metals and Its Application*, ch. 1, pp. 7–9. Oxford science publications, Clarendon Press, 1982.

[10] S. H. Carpenter and R. H. Wittman, "Explosion welding," *Annual Review of Materials Research*, vol. 5, no. Volume 5„ pp. 177–199, 1975.

[11] D. L. Olson, T. A. Siewert, S. Liu, and G. R. Edwards, *Welding, Brazing, and Soldering*, ch. N/A, pp. 524–525. ASM International, 01 1993.

[12] L. R. Carl, "Brass welds, made by detonation impulse," *Metal progress*, pp. 102–103, 1944.

[13] V. Philipchuk, "Explosive welding status," in *Creative Manufacturing Seminar. ASTME Paper*, pp. 65–109, 1965.

[14] J. S. Rinehart and J. Pearson, *Behavior of metals under impulsive loads*. American Society for Metals, 1954.

[15] J. S. Rinehart and J. Pearson, "Explosive working of metals," *(No Title)*, 1963.

[16] A. Holtzman and C. Rudershausen, "Recent advances in metal working with explosives," *Sheet Metal Industries*, vol. 39, p. 399, 1962.

[17] A. Deribas, V. Kudinov, and F. Matveenkov, "Effect of initial parameters on the process of wave formation in explosive welding," *J. Combust. Explos. Shock Waves*, vol. 3, no. 4, pp. 561–568, 1967. cited By 12.

[18] L. Zernow, I. Liberman, and W. Kincheloe, "Explosive welding, compaction, joining and perforation," in *Proceedings of the ASTME creative manufacturing seminars, SP*, pp. 60–141, 1961.

[19] A. Bahrani and B. Crossland, "Explosive welding and cladding," *An introductory survey and preliminary results, Proccedings of Instrumental Mechanical Engineering*, 1964.

[20] H. Otto and R. Wittman, "Evaluating of nasa-langley research center explosion seam welding," tech. rep., University of Denver for NASA-Langley Research Center, 1977.

[21] L. J. Bement, "Small-scale explosive seam welding," in *Proc. of the Symp. on Welding, Bonding, and Fastening*, 1972.

[22] B. Crossland and J. D. Will, "Explosive welding," tech. rep., Institute of Metals, 1970.

[23] M. D. Chadwick and P. W. Jackson, *Explosive Welding in Planar Geometries*, pp. 219–287. Dordrecht: Springer Netherlands, 1983.

[24] B. Crossland and A. S. Bahrani, "Fundamentals, of explosive welding," *Contemporary Physics*, vol. 9, no. 1, pp. 71–87, 1968.

[25] S. F. Jirdehi, S. G. Rad, S. Mazdak, and A. Alijani, "Proposing an analytical model for predicting the dimensions of interfacial waves produced in the explosive welding of coaxial cylinders," *Thin-Walled Structures*, vol. 190, p. 110982, 9 2023.

[26] J. B. Ribeiro, R. Mendes, and A. Loureiro, "Review of the weldability window concept and equations for explosive welding," *Journal of Physics: Conference Series*, vol. 500, p. 052038, may 2014.

[27] B. B. Sherpa and S. Saravanan, "Review of the weldability window in explosive welding processes," *Journal of Alloys and Metallurgical Systems*, vol. 9, p. 100150, 2025.

[28] R. H. Wittman, "The influence of collision parameters of the strength and microstructure of an explosion welded aluminium alloy," *Proc. 2nd Int. Sym. on Use of an Explosive Energy in Manufacturing Metallic Materials*, pp. 153–168, 1973.

[29] G. H. S. d. F. L. d. Carvalho, *Dissimilar Joining by Explosive Welding: Aluminium to Copper and Aluminium to Steel*. PhD thesis, 00500:: Universidade de Coimbra, 2019.

[30] G. Cowan, O. Bergmann, and A. Holtzman, "Mechanism of bond zone wave formation in explosion-clad metals," *Metallurgical and Materials Transactions B*, vol. 2, pp. 3145–3155, 1971.

[31] A. Burkhardt, E. Hornbogen, and K. Keller, "Transition to turbulent flow in crystals," *Z. Metallk.*, vol. 58, pp. 410–415, 1967.

[32] D. Jaramillo, A. Szecket, and O. T. Inal, "On the transition from a waveless to a wavy interface in explosive welding," *Materials Science and Engineering*, vol. 91, pp. 217–222, 1987.

[33] A. Vivek, B. Liu, S. Hansen, and G. Daehn, "Accessing collision welding process window for titanium/copper welds with vaporizing foil actuators and grooved targets," *Journal of Materials Processing Technology*, vol. 214, pp. 1583–1589, 2014.

[34] A. Vivek, S. Hansen, B. Liu, and G. S. Daehn, "Vaporizing foil actuator: A tool for collision welding," *Journal of Materials Processing Technology*, vol. 213, no. 12, p. 2304 – 2311, 2013. Cited by: 122.

[35] S. Salem, L. Lazari, and S. Al-Hassani, "Explosive welding of flat plates in free flight," *International Journal of Impact Engineering*, vol. 2, no. 1, pp. 85–101, 1984.

[36] H. Paul, W. Skuza, R. Chulist, M. Miszczyk, A. Gałka, M. Prażmowski, and J. Pstruś, "The effect of interface morphology on the electro-mechanical properties of ti/cu clad composites produced by explosive welding," *Metallurgical and Materials Transactions A: Physical Metallurgy and Materials Science*, vol. 51, pp. 750–766, 2 2020.

[37] G. H. Carvalho, R. Mendes, R. M. Leal, I. Galvão, and A. Loureiro, "Effect of the flyer material on the interface phenomena in aluminium and copper explosive welds," *Materials and Design*, vol. 122, pp. 172–183, 5 2017.

[38] V. Lysak and S. Kuzmin, "Energy balance during explosive welding," *Journal of Materials Processing Technology*, vol. 222, pp. 356–364, 2015.

[39] A. Deribas, "Physics of explosive hardening and welding," 1980.

[40] P. Shmorgun and Sonnov, "Calculation of the lower boundary of heterogenous metals explosive welding," *Explosive Welding and Properties of Welded Joints. Inter-Departmental Transaction, Volgograd polytechnic institute, Volgograd (1986)*, pp. 47–54, 1986.

[41] V. Belayev, D. Devoino, and V. Kasperovich, "On the lower boundary of explosive welding modes," *Poroshkovayametallurgiya*, vol. 2, pp. 51–56, 1978.

[42] V. Shmorgun, “On the evaluation of explosive welding efficient modes,” *Explosive Welding and Properties of Welded Joints. Inter-Departmental Transaction. Volgograd Polytechnic Institute, Volgograd*, pp. 68–74, 1988.

[43] V. Lysak and S. Kuzmin, “Explosive welding,” *N/A*, 2005.

[44] W. S. de Rosset and, “Analysis of explosive bonding parameters,” *Materials and Manufacturing Processes*, vol. 21, no. 6, pp. 634–638, 2006.

[45] Q. Zhou, J. Feng, and P. Chen, “Numerical and experimental studies on the explosive welding of tungsten foil to copper,” *Materials*, vol. 10, no. 9, 2017.

[46] A. DERIBAS, “Physics of explosive hardening and welding(russian book on physics of explosive hardening and welding covering high velocity inelastic collisions, shock wave generation, strengthening mechanisms of metals, etc),” *Novosibirsk, Izdatel’stvo Nauka, 1972. 188*, 1972.

[47] M. Yang, H. Ma, and Z. Shen, “Study on self-restrained explosive welding with high energy efficiency,” *International Journal of Advanced Manufacturing Technology*, vol. 99, pp. 3123–3132, 12 2018.

[48] Y. Wang, X. Li, X. Wang, and H. Yan, “Fabrication of a thick copper-stainless steel clad plate for nuclear fusion equipment by explosive welding,” *Fusion Engineering and Design*, vol. 137, pp. 91–96, 2018.

[49] Z. I. Efremov, V.V., “Determination of the upper limit to explosive welding.,” *Combust Explos Shock Waves 12, 226–230*, 1976.

[50] V. I. Kuz’min, V. I. Lysak, A. N. Kriventsov, and M. A. Y. and, “Critical conditions of the formation and failure of welded joints in explosive welding,” *Welding International*, vol. 18, no. 3, pp. 223–227, 2004.

[51] S. Reid, “Wake instability mechanism for wave formation in explosive welding,” *International Journal of Mechanical Sciences*, vol. 20, no. 4, pp. 247–253, 1978.

[52] J. M. Walsh, R. G. Shreffler, and F. J. Willig, “Limiting conditions for jet formation in high velocity collisions,” *Journal of Applied Physics*, vol. 24, pp. 349–359, 1953.

[53] G. R. Cowan and A. H. Holtzman, “Flow configurations in colliding plates: Explosive bonding,” *Journal of Applied Physics*, vol. 34, pp. 928–939, 1963.

[54] S. Saravanan and K. Raghukandan, “Weldability windows for explosive cladding of dissimilar metals,” *Advanced Materials Research*, vol. 445, pp. 729–734, 2012.

[55] A. Arab, Y. Guo, Q. Zhou, and P. Chen, “Joining alcocrfeni high entropy alloys and al-6061 by explosive welding method,” *Vacuum*, vol. 174, 4 2020.

[56] G. R. Abrahamson, “Permanent periodic surface deformations due to a traveling jet,” *Journal of Applied Mechanics*, vol. 28, pp. 519–528, 12 1961.

[57] G. H. Carvalho, I. Galvão, R. Mendes, R. M. Leal, and A. Loureiro, “Weldability of aluminium-copper in explosive welding,” *International Journal of Advanced Manufacturing Technology*, vol. 103, pp. 3211–3221, 8 2019.

[58] G. H. Carvalho, I. Galvão, R. Mendes, R. M. Leal, and A. Loureiro, “Explosive welding of aluminium to stainless steel using carbon steel and niobium interlayers,” *Journal of Materials Processing Technology*, vol. 283, 9 2020.

[59] G. H. Carvalho, I. Galvão, R. Mendes, R. M. Leal, and A. Loureiro, “Friction stir welding and explosive welding of aluminum/copper: process analysis,” *Materials and Manufacturing Processes*, vol. 34, pp. 1243–1250, 2019.

[60] G. H. Carvalho, I. Galvão, R. Mendes, R. M. Leal, and A. Loureiro, “Aluminum-to-steel cladding by explosive welding,” *Metals*, vol. 10, pp. 1–18, 8 2020.

[61] G. H. Carvalho, I. Galvão, R. Mendes, R. M. Leal, and A. Loureiro, “Formation of intermetallic structures at the interface of steel-to-aluminium explosive welds,” *Materials Characterization*, vol. 142, pp. 432–442, 8 2018.

[62] G. H. Carvalho, I. Galvão, R. Mendes, R. M. Leal, and A. Loureiro, “Microstructure and mechanical behaviour of aluminium-carbon steel and aluminium-stainless steel clads produced with an aluminium interlayer,” *Materials Characterization*, vol. 155, 9 2019.

[63] G. H. Carvalho, I. Galvão, R. Mendes, R. M. Leal, A. B. Moreira, and A. Loureiro, “The role of physical properties in explosive welding of copper to stainless steel,” *Defence Technology*, vol. 22, pp. 88–98, 4 2023.

[64] G. H. Carvalho, I. Galvão, R. Mendes, R. M. Leal, and A. Loureiro, “Explosive welding of aluminium to stainless steel,” *Journal of Materials Processing Technology*, vol. 262, pp. 340–349, 12 2018.

[65] G. H. Carvalho, I. Galvão, R. Mendes, R. M. Leal, and A. Loureiro, “Influence of base material properties on copper and aluminium–copper explosive welds,” *Science and Technology of Welding and Joining*, vol. 23, pp. 501–507, 8 2018.

[66] I. Galvão, G. H. Carvalho, J. Pimenta, T. Abreu, C. Leitão, R. M. Leal, and R. Mendes, “Structural analysis of aluminium-titanium-stainless steel three-layer composites produced by explosive welding,” *Welding in the World*, vol. 68, pp. 2911–2925, 11 2024.

[67] AZoM, “Aluminium alloy 5083 — properties, applications and processing,” 2025. Accessed 15 September 2025.

[68] E. Elango, S. Saravanan, and K. Raghukandan, “Experimental and numerical studies on aluminum-stainless steel explosive cladding,” *Journal of Central South University*, vol. 27, pp. 1742–1753, 6 2020.

[69] D. L. Olson, T. A. Siewert, S. Liu, and G. R. Edwards, *Welding, Brazing, and Soldering*. ASM International, 01 1993.